# Competitive Adsorption, Phase Segregation, and Molecular Motion at a Solid−Liquid Interface Studied by Scanning Tunneling Microscopy

**ARTICLE** *in* LANGMUIR · JUNE 1999

Impact Factor: 4.46 · DOI: 10.1021/la981658h



**4 AUTHORS**, INCLUDING:

David L Patrick
Western Washington University
**38** PUBLICATIONS **870** CITATIONS

# Competitive Adsorption, Phase Segregation, and Molecular Motion at a Solid−Liquid Interface Studied by Scanning Tunneling Microscopy

Robert T. Baker, Joseph D. Mougous, Andrew Brackley, and David L. Patrick*

*Department of Chemistry, Western Washington University, Bellingham, Washington 98225*

*Received November 30, 1998. In Final Form: April 9, 1999*

Binary mixtures of 4′-octyl-4-biphenylcarbonitrile (8CB) and *n*-tetracontane ($C_{40}H_{82}$) deposited as crystalline monolayers from a bulk fluid droplet on a graphite substrate were found to undergo nanometer-scale phase segregation into pure 8CB and pure alkane domains. Film morphology, molecular ordering, and domain motion were studied using scanning tunneling microscopy. Alkane adsorption was favored in the early stages of film growth, which was followed by a period of gradual annealing in which 8CB displaced alkane molecules from the surface. The structure and composition of the monolayer show that in films deposited from a bulk fluid with a 600:1 molar ratio of 8CB/*n*-tetracontane 8CB adsorption is thermodynamically favored. However, *n*-tetracontane had a significantly larger nucleation rate, leading to high alkane surface coverage shortly after film formation. Quantitative rate measurements of alkane domain replacement by 8CB have been made and correlated with the microscopic structure of the 8CB−alkane interface.

## Introduction

Competitive adsorption occurs whenever a multicomponent solution is brought into contact with an interface.[1] Because most liquids of practical interest are mixtures, competitive adsorption is a ubiquitous phenomenon. It plays an important role in systems as diverse as column chromatography,[2] drug-delivery vehicles and bioavailability,[3] and material transport in the environment.[4] Understanding how competitive phenomena influence the structure and composition of films deposited from liquid mixtures is therefore an important objective of fundamental and applied interest. Competitive adsorption involves a dynamic equilibrium between adsorbing species established through diffusion, adsorption, and desorption at the interface. The interplay between thermodynamic and kinetic factors that govern the properties of competitive adsorption can result in monolayer films with complex morphologies and a rich variety of dynamic phenomena with characteristic length and time scales spanning many orders of magnitude.

Systems which form ordered monolayers on solid substrates are particularly well-suited for studying competitive adsorption at nanometer length scales, because the monolayer structure can be directly investigated in situ using scanning probe microscopy.[5,6] This paper describes an investigation of adsorption from a two-component solution at a solid interface consisting of a liquid-crystal solvent [4′-alkyl-4-cyanobiphenyl (8CB), a room-temperature smectic A liquid crystal] and the paraffinic solute *n*-tetracontane ($C_{40}H_{82}$). These compounds were selected based on the results of previous studies which showed that each forms a crystalline monolayer and that dynamic motion within these monolayers occurs on a time scale discernible by scanning tunneling microscopy (STM) at room temperature.[7] We found that while partially miscible in the bulk, the two species phase-segregate when adsorbed on a graphite surface. Polycrystalline films deposited from this mixture evolved in structure and composition through motion of domain boundaries and gradual changes in the size and shape of existing domains.

## Experimental Section

Mixtures of 8CB and *n*-tetracontane were prepared in varying 8CB/$C_{40}H_{82}$ molar ratios from 98% pure samples (Aldrich Chemical Co., Inc.). Solutions were heated to ∼95 °C to homogenize the mixture and allowed to cool to room temperature prior to application to a substrate of highly oriented pyrolytic graphite (HOPG; ZYB-grade, Structure Probe Inc.). HOPG was baked at 650 °C in air for 5 min to remove residual organic adsorbates, then cooled, and cleaved immediately prior to usage. A (∼100 $\mu$L) droplet of the 8CB/*n*-tetracontane mixture was applied at room temperature or, in some cases, warmed slightly to facilitate spreading. The STM stylus penetrated the bulk fluid droplet to image molecules at the graphite interface. Mechanically cut Pt/Rh (87/13) or Pt/Ir (80/20) wire tips were used for imaging with a homebuilt STM. All images were acquired in constant-height mode and are presented unprocessed.

## Results and Discussion

**Film Morphology.** STM images showing the arrangement of molecules in pure 8CB and pure *n*-tetracontane films are presented in Figures 1 and 2. Both molecules form commensurate, crystalline monolayers.[8,11] The 8CB unit cell contains eight molecules, arranged so that the molecular dipoles cancel. It is the registration of the 8CB alkyl "tail" with the graphite substrate that appears to

* Corresponding author. Phone: (360) 650-3128. E-mail: patrick@chem.wwu.edu.

(1) Hall, D. G. *Thermodynamics of adsorption from dilute solutions*; NATO ASI Series C324; Plenum: New York, 1990; p 857.
(2) Giddings, J. C. *Unified Separation Science*; John Wiley: New York, 1991.
(3) Moudgil, B. M.; Prakash, T. S. *Colloids Surf., A* **1998**, *133*, 93.
(4) Murali, V.; Aylmore, L. A. G. *Soil Sci.* **1983**, *136*, 279.
(5) Frommer, J. *Thin Solid Films* **1996**, *273*, 112.
(6) Folkers, J. P.; Laibinis, P. E.; Whitesides, G. M.; Deutch, J. *J. Phys. Chem.* **1994**, *98*, 563. Tsao, M.-W.; Hoffmann, C. L.; Rabolt, J. F.; Johnson, H. E.; Castner, D. G.; Erdelen, C.; Ringsdorf, H. *Langmuir* **1997**, *13*, 4317. Rowe, G. K.; Creager, S. E. *Langmuir* **1994**, *10*, 1186. Stranick, S. J.; Parikh, A. N.; Tao, Y.-T.; Allara, D. L.; Weiss, P. S. *J. Phys. Chem.* **1994**, *98*, 7636. Stranick, S. J.; Atre, S. V.; Parikh, A. N.; Wood, M. C.; Allara, D. L.; Winograd, N.; Weiss, P. S. *Nanotechnology* **1996**, *7*, 438.
(7) Rabe, J. P.; Buchholz, S. *Phys. Rev. Lett.* **1991**, *66*, 2096.
(8) Foster, J. S.; Frommer, J. E. *Nature* **1988**, *333*, 542.

10.1021/la981658h CCC: $18.00 
Published on Web 06/04/1999

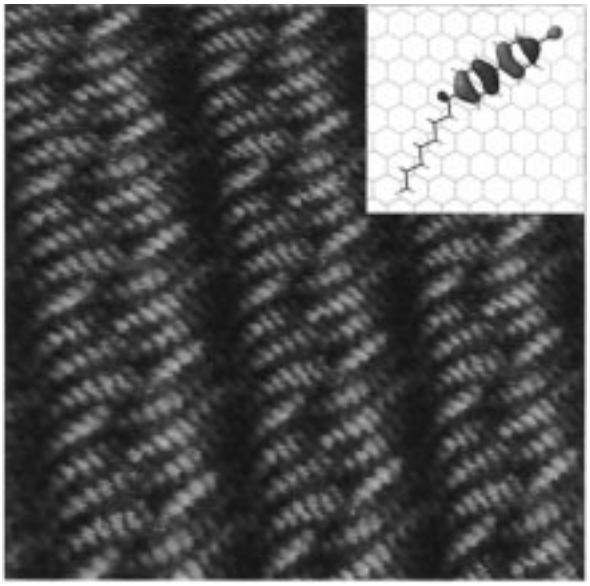

**Figure 1.** STM image of 8CB on HOPG. The image measures 12.8 nm × 12.8 nm ($I_{tunn}$ = 4.5 nA, $V_{bias}$ = −0.81 V). The inset shows the molecular structure of 8CB, along with its highest-occupied molecular orbital (HOMO). The HOMO was found via an ab initio Hartree−Fock calculation using a 6-31G* basis set for a gas-phase molecule whose geometry was minimized under the constraint that the alkyl tail lie in the plane of the biphenyl group.

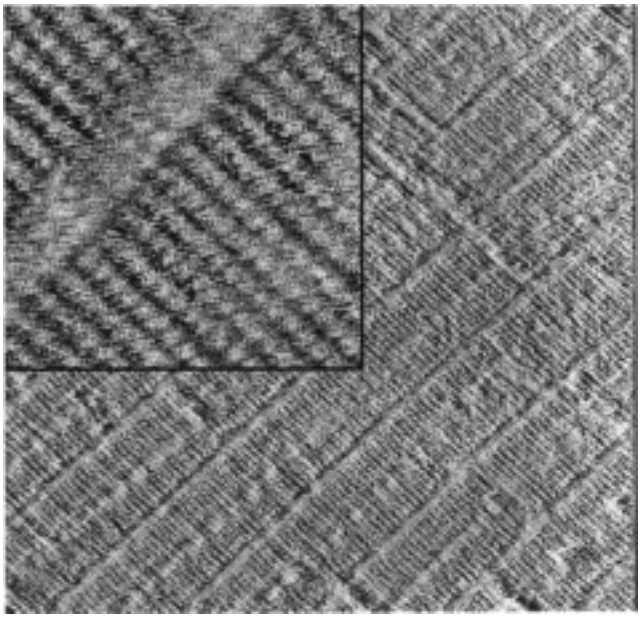

**Figure 2.** STM image of *n*-tetracontane on HOPG. The large image measures 34.0 nm × 35.0 nm ($I_{tunn}$ = 4.5 nA, $V_{bias}$ = −1.2 V). Each stick-shaped feature corresponds to one alkane molecule. The inset image measures 5.0 nm × 5.0 nm and shows the gap between lamellae.

produce a commensurate monolayer, with the tail orienting along one of three equivalent substrate lattice directions. The tunneling current is greatest above the cyanobiphenyl moiety, causing this portion of the molecule to appear bright in STM images. If the direction of electron tunneling is from the tip into the surface, the detailed appearance of each molecule approximates the regions of greatest electron density in the molecule's highest occupied molecular orbital,[9] as shown in the inset of Figure 1. When 8CB adsorbs to graphite, rotation about the C−C bond linking the cyanobiphenyl "head" group to the tail becomes strongly hindered. Consequently, rotational symmetry about the long molecular axis is broken, and molecules effectively develop a new chiral center; as a result, monolayers of 8CB are chiral. The two chiral forms combined with the 6-fold substrate symmetry lead to a total of six observationally distinct orientations for 8CB domains.[10]

We imaged pure 8CB and alkane films for comparison to the mixtures which were the focus of this study. Films of the former were prepared by depositing the neat fluid, while pure alkane monolayers were grown by depositing *n*-tetracontane from a saturated solution of phenyloctane onto clean graphite. As reported previously,[11] pure *n*-tetracontane monolayers crystallize into rowlike patterns, with molecules oriented perpendicular to the lamellae. The molecular backbone orientationally aligns with the graphite substrate, leading to three observationally distinct domain orientations. The ordering influence of the substrate is thought to arise from a favorable match between the graphite interhexagon distance and the distance between 1,3-methylene groups along the chain, which promotes commensurate adsorption with chains in an all-trans conformation.[12]

Mixed monolayers of 8CB and *n*-tetracontane resulted when solutions of these molecules were applied to graphite. The monolayer composition varied according to the molar ratio of 8CB and *n*-tetracontane in solution, with 8CB/$C_{40}H_{82}$ molar ratios of ∼600:1 (3.2 mg $mL^{-1}$) producing mixed monolayers, while those prepared from ∼100:1 (19 mg $mL^{-1}$) mixtures gave essentially pure *n*-tetracontane. All results described in this paper were from samples prepared using a 600:1 solution. Films prepared from the more concentrated alkane solution did not change in composition, while those prepared from dilute solutions did, as discussed below. Even in the case of the dilute 600:1 solution, the number of *n*-tetracontane molecules adsorbed to the surface (∼$10^{13}$) was small compared to the number in the fluid droplet (∼$10^{17}$), and therefore the bulk fluid composition was not appreciably affected by adsorption.

In solutions yielding mixed monolayers, *n*-tetracontane and 8CB underwent nanometer-scale phase segregation, forming domains of pure 8CB and pure *n*-tetracontane. Molecular order within each type of domain was identical with that found in the pure systems. Rather remarkably, however, we found that epitaxial ordering which was always observed in pure films of these two molecules was partially absent in films deposited as mixtures. In pure films registry of molecules with HOPG leads to a discrete set of domain orientations.[13] Working from models based on the structure of pure films, one predicts that there should be three observationally distinct intersection angles between rows of 8CB and rows of *n*-tetracontane at 18°, 42°, and 78°. Measurement of the row intersection angle between 8CB/*n*-tetracontane domain pairs in mixed systems showed that these values do occur but that other angles not expected based on the structure of pure systems are observed as well. This is shown in the histogram of intersection angles given in Figure 3, which contains results from 78 domain pairs. Intersection angles were measured between domains which shared the same

(9) Smith, D. P. E.; Horber, J. K. H.; Binnig, G.; Nejoh, H. *Nature* **1990**, *344*, 641.

(10) Smith, D. P. E. *J. Vac. Sci. Technol.* **1991**, *B9*, 1119.

(11) McGonigal, G. C.; Bernhardt, R. H.; Thomson, D. J. *Appl. Phys. Lett.* **1990**, *57*, 28.

(12) Groszek, A. J. *Proc. R. Soc. Lond. A* **1970**, *314*, 473.

(13) Patrick, D. L.; Morse, M. D.; Cee, V. J.; Beebe, T. P., Jr. *J. Phys. Chem. B* **1999**, in press.

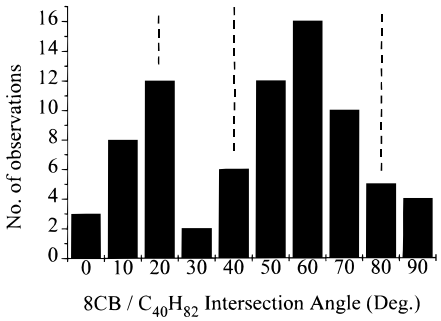


**Figure 3.** Histogram of 8CB/*n*-tetracontane row−row intersection angles. Values expected based on the monolayer structure of pure films of each molecule are shown as dashed lines.

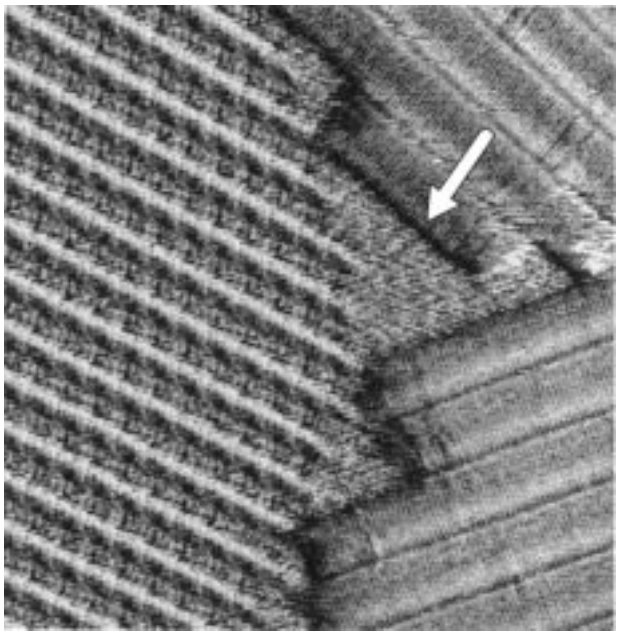

**Figure 4.** STM image of 8CB/*n*-tetracontane domain boundaries showing a region too small to accommodate ordered molecules. The image measures 42 nm × 44 nm ($I_{tunn}$ = 1.53 nA, $V_{bias}$ = −0.50 V). Two *n*-tetracontane domains are shown intersecting 8CB and each other. The detailed appearance of 8CB is somewhat different from that in Figure 1 in part because imaging conditions were optimized for *n*-tetracontane, not 8CB.

graphite terrace or adjacent graphite terraces, from images such as the one in Figure 4, to ensure that the substrate orientation was identical at both locations. In Figure 4 two *n*-tetracontane domains and one 8CB domain intersect, and all three intersection angles are in agreement with predictions from pure systems.

The data in Figure 3 provided two unexpected results. First, the range of intersection angles was greater than anticipated, with the distribution being much broader than those measured in pure 8CB and pure *n*-tetracontane films. Second, the most probable intersection angles did not coincide with those predicted from the structure of pure systems. In cases where the row intersection angle did not agree with predictions based on pure monolayer structures, the discrepancy was consistently found to arise from a misorientation of the *n*-tetracontane domain. In pure *n*-tetracontane films, molecular rows oriented exclusively at 0° and ±120° with respect to the substrate. However, in mixed films a wide range of orientations was observed: in some cases the orientation of *n*-tetracontane lamellae varied smoothly, following a curved or wavy path around substrate defects and 8CB domains. An example

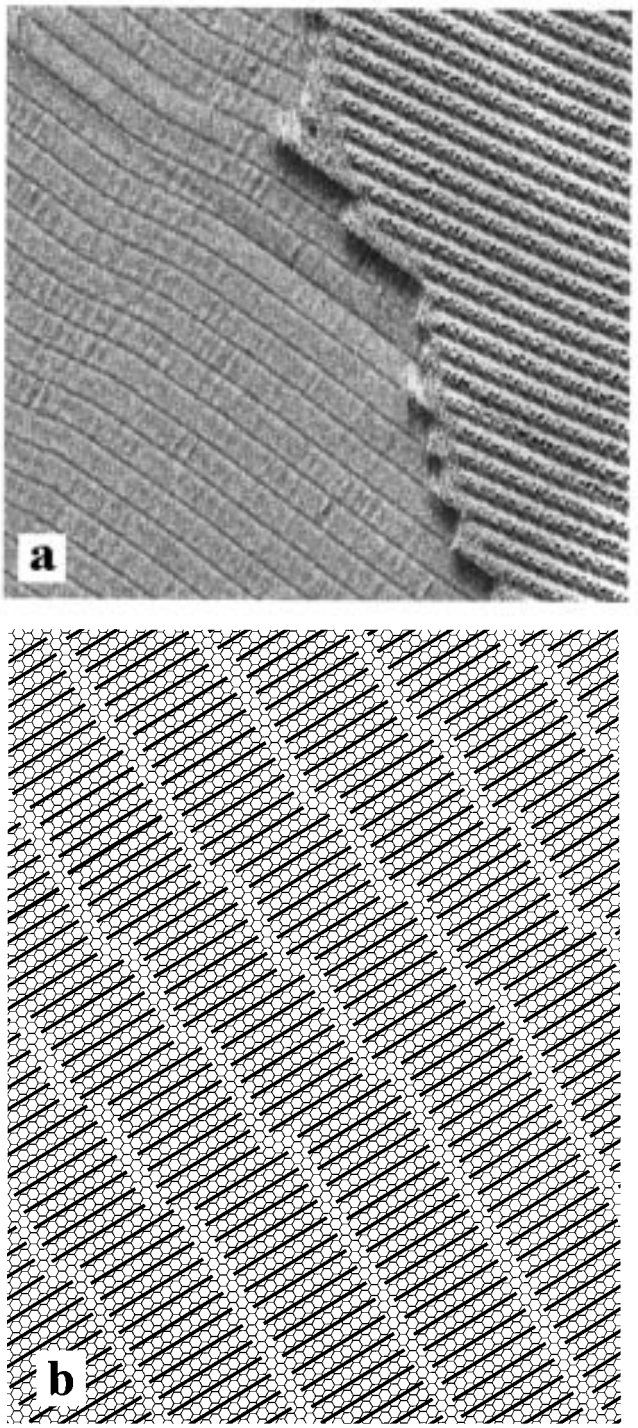


**Figure 5.** (a) *n*-Tetracontane lamellae are normally linear in pure films but in mixed monolayers frequently develop bent or wavy patterns (left-hand side). The domain on the right is 8CB. The image measures 90 nm × 88 nm. (b) Row curvature arises from incremental displacements in the position of alkane molecules perpendicular to the lamellae. *n*-Tetracontane molecules in the model are represented as solid lines and are not drawn to scale with the graphite substrate.

is shown in Figure 5a. This type of defect pattern is uncommon in pure alkane films, except close to their melting point,[14] but was frequently observed in mixed monolayers. Conversely, the arrangement of 8CB molecules never differed from the structure reported in pure

(14) Askadskaya, L.; Rabe, J. P. *Phys. Rev. Lett.* **1992**, *69*, 1395. Bucher, J.-P.; Roeder, H.; Kern, K. *Surf. Sci.* **1993**, *289*, 370. Ishida, K.; Taki, S.; Okabe, H.; Matsushige, K. *Jpn. J. Appl. Phys.* **1995**, *34*, 3846.

systems. These examples of nonepitaxial ordering were apparently driven by the (small) improvement it provided in packing efficiency, which was made more important in mixed monolayers because of the large number of irregularly shaped domain boundaries; when molecular rows were perfectly straight, regions developed at domain interfaces which were too small or incorrectly shaped for ordered molecules to fit properly (see below). Curved rows and nonepitaxial order leads to a modest reduction in the total surface area of these regions, allowing more of the surface to be covered by an ordered monolayer.

Changes in row orientation took place via incremental displacements of *n*-tetracontane molecules perpendicular to the lamellae, as shown in Figure 5b. The energy increase associated with these displacements is small, for two reasons: First, the ~2% mismatch between the spacing of alkane 1,3-methylene groups ($d = 0.254$ nm) and the interhexagon graphite spacing ($d = 0.246$ nm) results in a slight intramolecular misregistry that increases with chain length. Thus, if the terminal methyl group at one end of an *n*-tetracontane molecule were centered above a graphite hollow site, the other end of the chain would be displaced from the nearest hollow by ~0.16 nm, more than half the graphite period. This property of *n*-alkane adsorbates on HOPG results in a gradual decrease in the barrier toward translational motion with increasing chain length. *n*-Tetracontane is among the longest *n*-alkanes studied on HOPG by STM, and so it is not surprising to find an enhanced degree of chain mobility perpendicular to the row direction. This effect is negligible for 8CB, which has a comparatively short chain length. Second, a small translation in chain position amounts to a minor overall change in the number of intermolecular contacts between adjacent molecules, because only the chain ends are affected and only in molecules at the bend site (Figure 5b).

Near 8CB/*n*-tetracontane domain boundaries two unique types of molecular ordering were observed, depending on the relative orientation of molecular rows in the two domains. When rows intersected at angles much different from 0° or 90°, nanometer-sized regions occurred which were too small to accommodate crystalline packing. An example of this is shown in Figure 4, indicated by an arrow. Molecules in these regions were not individually resolved by STM, indicating they were undergoing rapid diffusive motion on the time scale of STM imaging. Adsorbates in these regions may be thought of as comprising a distinct "boundary phase", exhibiting structural and dynamic properties strikingly different from crystalline domains elsewhere on the surface. The formation of this phase appeared to be driven by molecular packing constraints. It was also common to observe small fluctuations in domain boundary shape and position on the order of one unit cell in size at these sites, indicating rapid exchange of molecules between the surface and solution. Below we draw a connection between nanometer-scale interface roughness and the overall rate of domain boundary motion.

When 8CB and *n*-tetracontane intersected at row angles near 0° or 90°, a different type of molecular order was observed near the boundary. An example is shown in Figure 6. Crystallinity in the *n*-tetracontane domain on the left was perfectly preserved right up to the interface; however, 8CB molecules immediately near the boundary on the right were disordered and not well-resolved in the image compared to 8CB molecules far from the boundary, indicating they were undergoing motion during image acquisition (i.e., 8CB appeared frizzy near the boundary). The disorder persisted even when the direction of tip scanning was changed by 90°, demonstrating it was not an artifact caused by the scan direction. This phenomenon cannot be entirely explained by molecular packing constraints, as the degradation in crystalline order extends 5−10 nm into the 8CB domain. Ordering of 8CB molecules at the interface may be affected by contact with adsorbed *n*-tetracontane or by impurities present but not directly imaged at the interface. A similar reduction in crystallinity at 8CB/8CB boundaries was found by Patrick et al. in a study of pure 8CB films.[19]

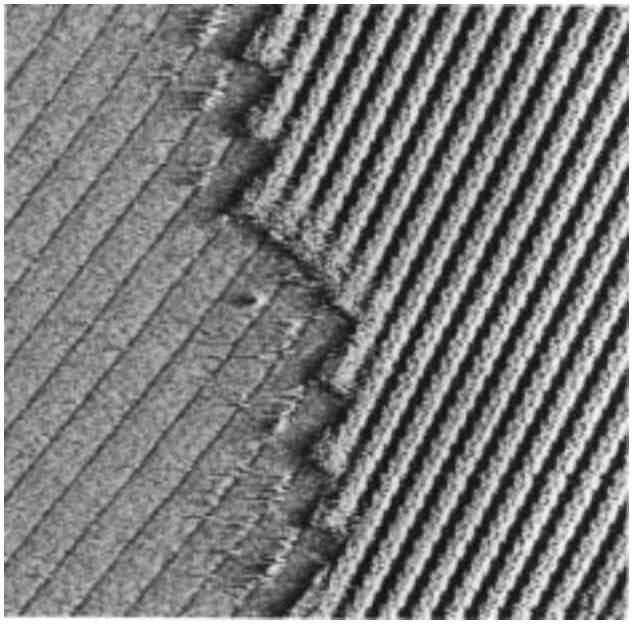

**Figure 6.** STM image of an 8CB/*n*-tetracontane domain boundary showing molecular disorder at the edge of the 8CB domain. The image measures 75 nm × 75 nm ($I_{tunn} = 1.9$ nA, $V_{bias} = -0.70$ V).

**Annealing Process.** Films prepared from a 600:1 solution initially showed high *n*-tetracontane coverage, which gradually decreased over a period of 1−2 days, eventually leaving a monolayer of nearly pure 8CB. Shortly after deposition, graphite terraces were largely covered by a polycrystalline mosaic of *n*-tetracontane domains whose average size was ~$10^4$ nm$^2$. Small 8CB domains which were also present initially gradually increased in size, replacing *n*-tetracontane. The fully annealed film consisted of large crystalline 8CB domains whose extent was limited by the size of the terraces and small pockets of *n*-tetracontane confined near substrate defects.

A set of images illustrating this process is presented in Figure 7. The first image was acquired 1 h after deposition, at a time when the surface coverages of 8CB and *n*-tetracontane were approximately equal. Numerous nanometer-sized domains occupied a single graphite terrace, with a prominent substrate defect providing a stationary point of reference. Subsequent images were acquired at 1.7 min intervals, revealing a gradual evolution in monolayer structure and composition leading ultimately to a single large 8CB domain bordered by smaller regions of *n*-tetracontane. Three distinct phases are present in the first frame: crystalline 8CB and *n*-tetracontane domains as well as smaller, semicrystalline regions bounded by ordered phases. Several of the latter are labeled S in the image. Unlike crystalline 8CB and *n*-tetracontane domains, molecules in these regions did not display uniform long-range order, although a certain degree of structure is evident over short distances. These semicrystalline domains were rapidly replaced by crystalline 8CB or *n*-tetracontane, making it difficult to establish the identity of molecules in these regions. By the second

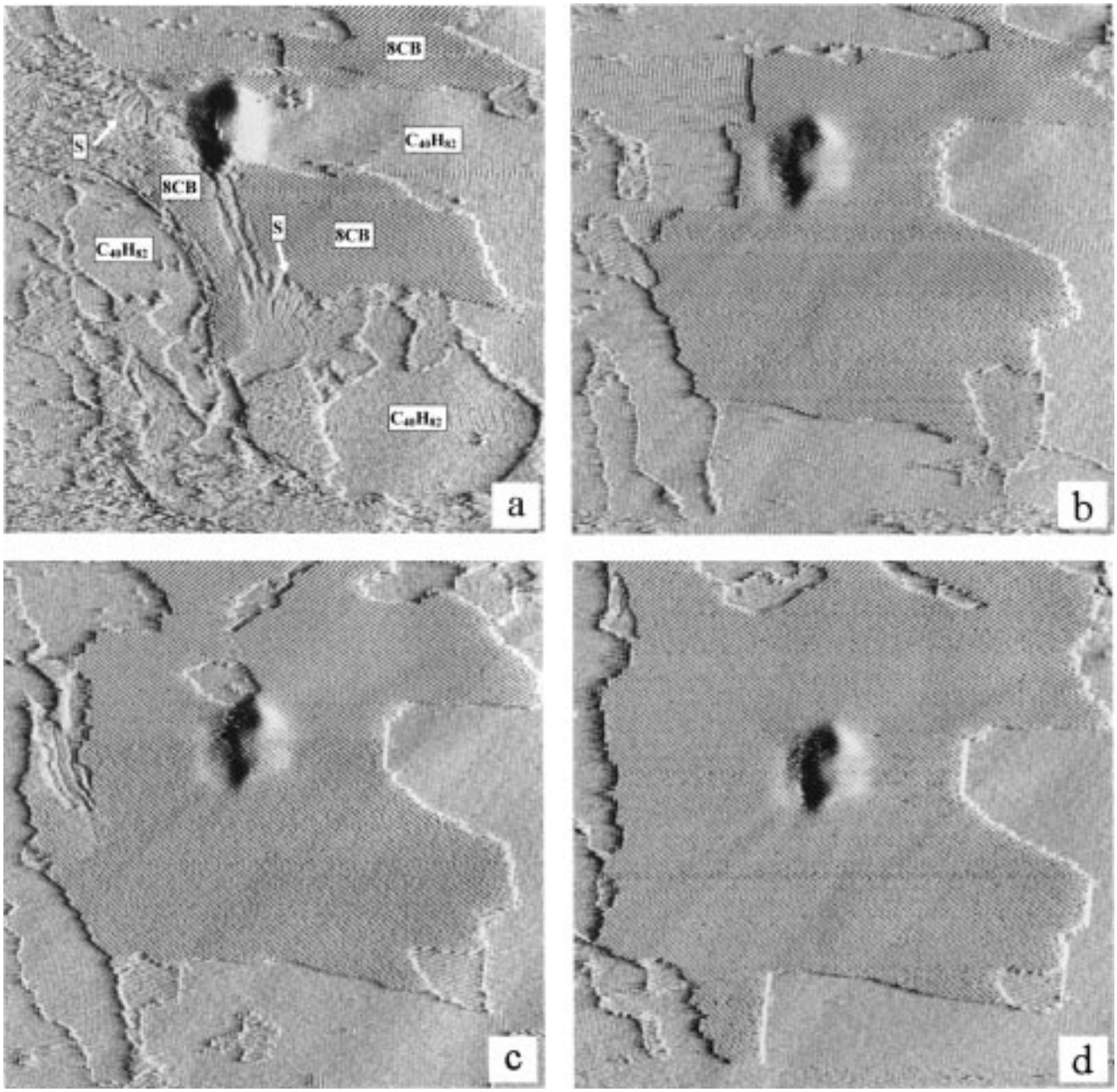


**Figure 7.** Films deposited from 8CB/*n*-tetracontane mixtures initially formed multiple, nanometer-sized domains of three distinct types: crystalline 8CB, crystalline *n*-tetracontane, and smaller regions of undetermined composition with semicrystalline order. Two domains of the latter are labeled S in part a. This stage of film formation was followed by a period of gradual annealing involving coalescence of small domains and an increase in 8CB surface coverage (parts b−d). The prominent feature near the top center of the images is a substrate defect. The interval between frames was 1.7 min. Images measure 460 nm × 460 nm ($I_{tunn}$ = 4.9−5.8 nA, $V_{bias}$ = −0.70 V).

frame few such domains remained. Over time the number and size of 8CB and *n*-tetracontane domains gradually changed until a single 8CB domain covered nearly the entire terrace (not shown).

We made the following general observations about the annealing process, based on this and numerous other examples from several different samples: First, 8CB coverage generally increased over time while *n*-tetracontane coverage decreased, although local fluctuations in surface coverage sometimes favored *n*-tetracontane. The overall trend toward increasing 8CB coverage showed that the initial monolayer composition was dominated by kinetic, rather than thermodynamic, factors and that crystalline 8CB was the surface phase with the lowest free energy. The composition of a fully annealed (equilibrium) film is related to the difference in the free energy of the adsorbed components.[15] The free energy change associated with adsorption and monolayer formation contains contributions from intermolecular interactions and adsorbate−substrate interactions through the heats of solvation and adsorption as well as contributions from the loss of conformational entropy and the entropy of mixing. The latter is the principle factor which causes the equilibrium surface composition to vary with changes in the composition of the bulk fluid. In films prepared from 600:1 solutions, 8CB was the more thermodynamically stable surface species (i.e., the species with the lowest free energy per unit area of surface), whereas in films

(15) Adamson, A. W. *The Physical Chemistry of Surfaces*, 3rd ed.; Wiley: New York, 1976.

prepared from 100:1 solutions, adsorption of *n*-tetracontane was thermodynamically favored.

The polydomain morphology which developed during deposition was quite similar in structure to the one formed when pure *n*-tetracontane monolayers were deposited from phenyloctane but very different from that formed by pure 8CB. At room temperature surface films of pure 8CB are composed of a small number of large domains (typically one per terrace). The initial film morphology is largely determined by the ratio of the growth rate to the nucleation rate, $\gamma = R_G/R_N$. For 8CB, $\gamma$ is large, so that on average there is time enough only for a single domain to nucleate on each terrace before coverage is complete. By comparison, $\gamma$ is small for *n*-tetracontane, leading to a large number of small domains. The morphology of mixed 8CB/*n*-tetracontane monolayers is therefore consistent with the kinetics of film formation in the pure systems only if the nucleation rate of *n*-tetracontane is greater than that of 8CB, i.e., $R_N^{C_{40}H_{82}} > R_N^{8CB}$; if the reverse were true, a single large 8CB domain would form initially and the polydomain structure would never develop. Nucleation rates are determined by a combination of kinetic and thermodynamic factors,[16] but it is reasonable to expect some correlation between the complexity of the unit cell and the rate of nuclei formation. Energetic factors being equal, a complex unit cell would take longer to form, and to the extent that nuclei resemble the unit cell, the nucleation time would be correspondingly increased. The conclusion $R_N^{C_{40}H_{82}} > R_N^{8CB}$ qualitatively agrees with this expectation because the unit cell of *n*-tetracontane consists of a single fully elongated molecule while the unit cell of 8CB contains eight molecules in a comparatively complex arrangement.

The rate of change of film morphology and composition was greatest during the initial stages of annealing. This was because change occurred through boundary motion, and in the initial stages of annealing there were more domains and more total boundary length. As annealing proceeded, the number of domains per unit area of substrate diminished, leading to larger, generally more compact, crystallites with less boundary length.

We found that 8CB growth always occurred at the edges of *n*-tetracontane crystallites via an increase in size of existing 8CB domains; 8CB was never observed to form new nuclei in the center of an *n*-tetracontane domain, or at step edges or other defect sites. This observation is understood by considering that a minimum surface area is required for an 8CB germ to reach critical growth size and become a nucleus, which is at least the size of one unit cell and probably much larger.[17] Following the initial period of film formation, very little surface area remained uncovered by a crystalline monolayer. For new 8CB nuclei to form, adsorbed molecules would therefore need to be displaced, a process which presents a large barrier to the initiation of new nuclei.

The crystallographic orientation of 8CB was perfectly preserved during growth, and appeared not to be influenced by the orientation of molecules in the *n*-tetracontane domain. At first this finding may seem surprising, in view of high-resolution images showing significant alterations in 8CB molecular order at 8CB/*n*-tetracontane interfaces (e.g., Figure 6). However, if the orientation of 8CB domains underwent periodic changes during growth, a corresponding number of new 8CB/8CB domain boundaries would be generated. The line tension associated with these boundaries is rather large,[18] so that it is more favorable to propagate an existing domain than it is to generate a new one.

We also observed that the rate of 8CB domain growth was proportional to the molecular-scale roughness of the 8CB/*n*-tetracontane interface. To quantify this relationship, we followed changes in domain size of *n*-tetracontane regions bordered only by 8CB and one or more graphite steps. An example is presented in Figure 8, which shows frames from a sequence of images acquired at 7.9 min intervals. Additional frames spaced more closely in time were also acquired but are not shown in the figure. The entire series covered a 79 min time period. Lines drawn in the images indicate the locations of the 8CB/*n*-tetracontane boundary in the prior frame. In this example an *n*-tetracontane domain was bordered on the left and right by 8CB and on the top and bottom by HOPG step defects. Other substrate defects passing through the center of the *n*-tetracontane domain appeared not to influence domain boundary motion. In films of pure 8CB, substrate steps and other defects strongly pin 8CB/8CB domain boundaries, inhibiting their motion.[18] However, we observed no such pinning for 8CB/*n*-tetracontane boundaries.

The right-hand 8CB domain steadily encroached upon the *n*-tetracontane domain, eventually replacing it entirely, along with the 8CB domain on the left. The 8CB domain on the left initially advanced very slowly, then reversed its motion, and began to recede. At the end of the process, the *n*-tetracontane domain rapidly diminished in size as the 8CB domain on the right swept across the region, replacing both *n*-tetracontane and the left-hand 8CB domain.

In most cases where 8CB replaced *n*-tetracontane, the rate of motion of the boundary separating the two domains was clearly related to the roughness of the 8CB/*n*-tetracontane interface. Boundaries which were straight and ran parallel to *n*-tetracontane lamellae, such as the left-hand boundary in Figure 8, were markedly more stable than those which were stepped, such as the right-hand boundary. Once a smooth boundary formed, motion occurred much more slowly, or not at all.

This relationship between the rate of domain boundary motion and interface roughness is shown in Figure 9, which contains data from all images of the sequence up to $t =$ 59 min. The plot shows the area change due to motion of the right-hand 8CB/*n*-tetracontane boundary between successive frames. The "roughness" of the interface was measured in terms of the number of steps, $N_c$, which occurred along the right-hand 8CB/*n*-tetracontane boundary. The size of these steps equaled the width of the *n*-tetracontane lamellae, and they were easily discerned in full-size images. To distinguish area changes due to motion of the left- and right-hand boundaries, the area change was measured relative to a fixed position in the center of the *n*-tetracontane domain. Figure 9 shows that the rate of domain boundary motion is correlated with the boundary's roughness as measured by the parameter $N_c$. A similar relationship was observed for other domain boundaries and other intersection angles.

Irregular interfaces led to an abundance of sites where geometric constraints preclude crystalline ordering, like the region indicated by an arrow in Figure 4. The correlation between the rate of domain boundary motion and interface roughness suggests that these sites play an important role in promoting boundary movement. Smooth, straight 8CB/*n*-tetracontane interfaces had few such sites,

(16) Strickland-Constable, R. F. *Kinetics of Mechanism of Crystallization*; Academic Press: New York, 1968.

(17) Patrick, D. L.; Cee, V. J.; Beebe, T. P., Jr. *Science* **1994**, *265*, 231.

(18) Patrick, D. L.; Cee, V. J.; Purcell, T.; Beebe, T. P., Jr. *Langmuir* **1996**, *12*, 1830.

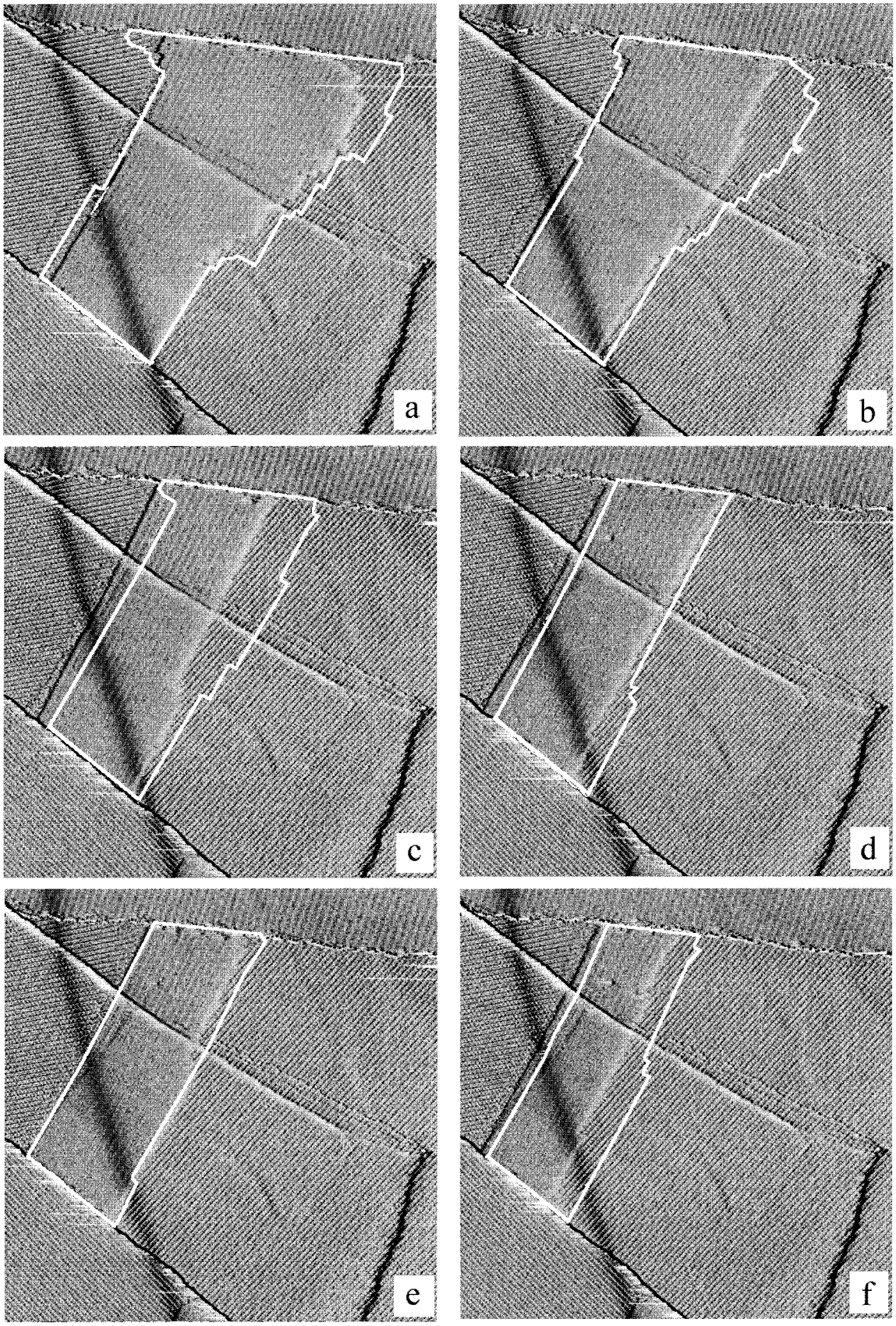


**Figure 8.** Portion of a set of 21 sequential images showing changes in the size and shape of an *n*-tetracontane domain bounded on the top and bottom by substrate step defects and on the left and right by 8CB. Additional images were acquired spaced more closely in time but are not shown in the figure. The solid white line indicates the position and shape of the *n*-tetracontane domain in the immediately preceding frame. The 8CB domain on the right gradually replaced *n*-tetracontane and ultimately the 8CB domain on the left as well. The images measure 250 nm × 250 nm and are separated by 7.9 min ($I_{tunn}$ = 1.1−1.6 nA, $V_{bias}$ = −0.52 V).

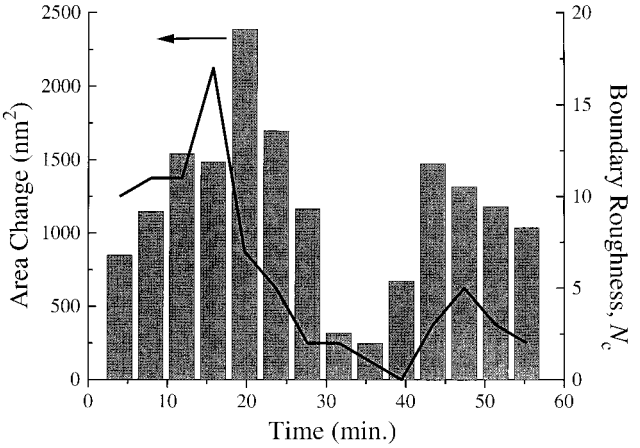


**Figure 9.** The rate of motion of 8CB/*n*-tetracontane domain boundaries is related to the roughness of the interface. The plot shows changes in the size of the *n*-tetracontane domain in Figure 8 along with the instantaneous roughness of the right-hand 8CB/*n*-tetracontane boundary for the full sequence of images in Figure 8. The area change is from movement of the right-hand boundary only.

which may explain why motion took place slowly at these boundaries.

Three distinct steps occurred during the type of domain boundary motion shown in Figure 9, which involved growth of an 8CB domain and loss of *n*-tetracontane. These are (1) desorption of *n*-tetracontane, (2) diffusion to the surface and adsorption of 8CB, and (3) molecular orientation and incorporation of 8CB into the crystalline 8CB domain. The last step is known to occur very rapidly in pure 8CB films from previous studies that have described rare cases where nucleation on an uncrystallized surface occurred during image acquisition. In those examples growth was completed across the entire scan area in a few milliseconds, corresponding to a linear growth rate of at least $10^3$ nm $s^{-1}$.[19] The rate of 8CB domain growth is therefore reduced in mixed systems compared to pure systems by at least 3−5 orders of magnitude. The rate of the second step, which involves material transport to the surface and 8CB adsorption, cannot significantly differ from that in pure systems because the fluid was overwhelmingly concentrated in 8CB. The rate-limiting step in 8CB domain growth must therefore arise from the first step, desorption of *n*-tetracontane molecules. These results suggest that *n*-tetracontane desorption occurs more readily at disordered boundary sites than elsewhere along the interface. The barrier to desorption may be reduced because molecules at these sites may not be adsorbed along their entire length (as they are in crystalline regions). Irregular packing also leads to a reduction in the number of favorable intermolecular contacts between adsorbed molecules compared to those in crystalline regions, which would also reduce the barrier to desorption (by raising the surface energy of adsorbed molecules).

While interface roughness was clearly related to the rate of boundary motion, it was evident that additional factors were important, such as the perturbing influence of the tip and the overall size of the two domains. When *n*-tetracontane domains shrunk below a certain threshold size (roughly 50 nm in diameter), 8CB growth sometimes accelerated, with 8CB replacing all of the remaining *n*-tetracontane molecules in a single event too rapid to follow with STM. An event of this kind occurred at the end of the sequence shown in Figure 8. Similarly, very small 8CB domains bordered by a larger *n*-tetracontane domain were sometimes suddenly replaced by *n*-tetracontane. Accelerated reduction in the size of small domains may occur because small domains possess large perimeter/area ratios and hence a higher total surface energy per unit area than large domains. If so, rapid elimination of small domains would follow a mechanism similar to Ostwald ripening, which is thermodynamically driven by a reduction in surface energy (or line energy, in two dimensions).[20] Another alternative, which is speculative, is that chemical interactions between solution-phase molecules and the crystalline monolayer may cause fluid layers immediately adjacent to the interface to become locally enriched in the type of molecule adsorbed to the surface. Fluid films adjacent to solid surfaces are known to possess structures intermediate between solid and liquid states, so that intermolecular interactions and molecular packing factors similar to those that cause phase segregation in the crystalline monolayer may also affect local fluid composition.[21] Concentration gradients have been observed in computer simulations of fluid alkane films deposited from mixtures of varying chain length.[22] If the fluid above the monolayer were to become locally enriched in one molecule, the equilibrium surface concentration would shift in favor of that molecule.[23] This would result in accelerated elimination of small domains of one type by large domains of another as the local fluid composition became increasingly enriched in the type of molecule present in the larger domain.

## Summary

We have reported the structure and composition of monolayer films deposited from a mixture of *n*-tetracontane and 8CB. Competitive adsorption initially favors *n*-tetracontane, which formed a polycrystalline monolayer covering most of the surface. A smaller number of 8CB domains gradually increased in size over a period of days by growth of existing nuclei. 8CB domain growth was found to be associated with small regions of disordered molecules along domain boundaries. The initial structure and composition of the films suggest that a high surface coverage of 8CB is thermodynamically favored but that the nucleation rate of *n*-tetracontane is significantly higher than that of 8CB.

**Acknowledgment.** We wish to thank Steven Hickman for his assistance. This research was supported by a Cottrell College Science Award from Research Corp. (CC4564) and a grant from the National Science Foundation (CHE-9504630).

LA981658H

(19) Patrick, D. L.; Cee, V. J.; Beebe, T. P., Jr. *J. Phys. Chem.* **1996**, *100*, 8478.

(20) Tomellini, M.; Fanfoni, M. In *Interfacial Science*; Roberts, M. W., Ed.; Blackwell Science: London, 1997.

(21) Nhushan, B.; Israelachvili, J. N.; Landman, U. *Nature* **1995**, *374*, 607.

(22) See, for example, Xia, T. K.; Landman, U. *Science* **1993**, *261*, 1310.

(23) Venkataram, B.; Breen, J. J.; Flynn, G. W. *J. Phys. Chem.* **1995**, *99*, 6608.